PHYSICAL REVIEW B **88**, 045323 (2013)

Anisotropic conductivity and weak localization in HgTe quantum wells with a normal energy spectrum

G. M. Minkov,[1,2] A. V. Germanenko,[2] O. E. Rut,[2] A. A. Sherstobitov,[1,2] S. A. Dvoretski,[3] and N. N. Mikhailov[3]
[1]*Institute of Metal Physics RAS, 620990 Ekaterinburg, Russia*
[2]*Institute of Natural Sciences, Ural Federal University, 620000 Ekaterinburg, Russia*
[3]*Institute of Semiconductor Physics RAS, 630090 Novosibirsk, Russia*
(Received 16 April 2013; published 30 July 2013)

The results of experimental study of interference induced magnetoconductivity in narrow quantum well HgTe with a normal energy spectrum are presented. Analysis is performed by taking into account the conductivity anisotropy. It is shown that the fitting parameter τ_ϕ corresponding to the phase relaxation time increases in magnitude with the increasing conductivity (σ) and decreasing temperature following the $1/T$ law. Such a behavior is analogous to that observed in the usual two-dimensional systems with a simple energy spectrum and corresponds to the inelasticity of electron-electron interaction as the main mechanism of the phase relaxation. However, it drastically differs from that observed in the wide HgTe quantum wells with the inverted spectrum, in which τ_ϕ, being obtained by the same way, is practically independent of σ. It is presumed that a different structure of the electron multicomponent wave function for the inverted and normal quantum wells could be the reason for such a discrepancy.

DOI: 10.1103/PhysRevB.88.045323 PACS number(s): 73.20.Fz, 73.21.Fg, 73.63.Hs

I. INTRODUCTION

Two-dimensional systems based on gapless semiconductors HgTe are unique objects. HgTe is a semiconductor with inverted orderings of Γ_6 and Γ_8 bands. The Γ_6 band, which is the conduction band in the usual semiconductor, is located in HgTe lower in energy than the degenerate at the $k = 0$ band Γ_8, where k is a quasimomentum. So unusual positioning of the bands leads to crucial features of the electron and hole spectrum under space confinement.[1–4] For instance, at some critical quantum well width $d = d_c \simeq 6.5$ nm, the energy spectrum is gapless and linear.[5] In the wide quantum wells $d > d_c$, the lowest electron subband is mainly formed from the Γ_8 states at a small quasimomentum value, while the Γ_6 forms the hole states in the depth of the valence band. Analogous to the bulk material, such a band structure is referred to as inverted structure. At $d < d_c$, the band ordering is normal. It is analogous to that in conventional narrow-gap semiconductors; the highest valence subband at $k = 0$ is formed from the heavy hole Γ_8 states, while the lowest electron subband is formed both from the Γ_6 states and from the light Γ_8 states.

The energy spectrum and specifics of transport phenomena in HgTe based heterostructures were studied intensively in last decade both experimentally[6–12] and theoretically.[5,13–15] Specifics of the electron interference, weak localization, and antilocalization were studied mainly theoretically for the range of parameters where the energy spectrum is close to the Dirac type.[13,15] The authors of Ref. 15 performed a most detailed symmetry analysis of a 2D electron system in a HgTe quantum well and showed that the temperature and magnetic field dependencies of the interference induced magnetoresistance are of a great variety. They can be localizing, antilocalizing, or can demonstrate the crossover from one type to another one depending on the symmetry of the perturbation and parameters of the Hamiltonian.

Experimentally, the interference contribution to the conductivity in two-dimensional HgTe heterostructures was studied in two papers only.[16,17] Single quantum wells with 2D electron gas were investigated in both papers. The authors of Ref. 16 merely demonstrated that the interference induced low-field magnetoresistivity is observed both in narrow ($d < d_c$) and in wide ($d > d_c$) quantum wells. More detailed studies were carried out in Ref. 17, however only structures with inverted spectrum $d = (9–10)$ nm were investigated. There it was found that the temperature dependencies of the fitting parameter τ_ϕ corresponding to the phase relaxation time is plausible, it is close to $1/T$ law. However, τ_ϕ remains practically independent of the conductivity over the wide conductivity range $(3–130)\, G_0$, where $G_0 = e^2/\pi h$. This finding is in conflict with theoretical arguments[18] and experimental data for conventional 2D systems with a simple energy spectrum,[17] in which τ_ϕ is enhanced with the conductivity. This fact calls into question the adequacy of the use of the standard expressions for description of the interference induced magnetoresistance in the structures with inverted spectrum. Another possible reason for the conflict is specific to the phase relaxation in the type of structures. The study of the interference induced magnetoresistance in the HgTe quantum wells with normal spectrum ($d < d_c$) can shed some light on this issue.

II. EXPERIMENTAL DETAILS

The HgTe quantum wells were realized on the basis of a HgTe/$Hg_{1-x}Cd_xTe$ ($x = 0.65$) heterostructure grown by molecular beam epitaxy on a GaAs substrate with the (013) surface orientation.[19] The nominal width of the quantum well was $d = 5$ nm. The architecture of the heterostructure, the energy diagram, and dispersion law $E(k)$ calculated in the 6×6 **kP** model with the use of the direct integration technique as described in Ref. 20 are shown in Fig. 1. The parameters from Refs. 21 and 22 have been used. The samples were etched into the Hall bars. The measurements were performed on two types of bars. The first type was the standard bar shown in Fig. 2(a), the second one was the L-shaped two-arm Hall

 ©2013 American Physical Society

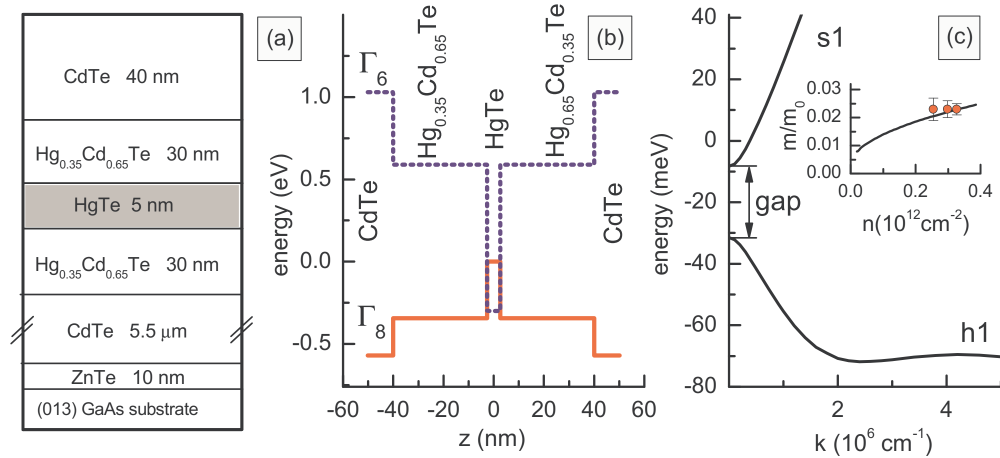

FIG. 1. (Color online) (a) Architecture and (b) energy diagram of the structure under investigation. (c) The dispersion for the lowest electron ($s1$) and highest hole ($h1$) subbands calculated in the framework of the isotropic 6×6 **kP** model. The inset shows the electron density dependence of the effective mass for the electron subband $s1$. Symbols plot the data, and the line shows the calculated dependence.

bar schematically depicted in Fig. 3. The width of the bars (B) and the distance between the potential probes (L) are the same and consists of 0.5 mm. To change the electron density (n) in the quantum well, the field-effect transistors were fabricated with parylene as an insulator and aluminum as a gate electrode. Measurements were taken at temperatures of 1.3–4.2 K. All the data will be presented for $T = 1.35$ K, unless otherwise specified. The electron effective mass needed for the quantitative interpretation was determined from the analysis of the temperature behavior of the Shubnikov–de Haas (SdH) oscillations. It is approximately equal to $0.023\,m_0$ within the range $n = (2.5\text{–}3.3) \times 10^{11}$ cm^{-2}. These data agree well with theoretical results obtained in the **kP** model [see inset in Fig. 1(c)]. For lower electron density $n < 2.5 \times 10^{11}$ cm^{-2} we employ the theoretical m vs n dependence.

III. RESULTS AND DISCUSSION

The gate voltage (V_g) dependence of the electron density (found both from the Hall effect and from the SdH oscillations) and conductivity are plotted in Figs. 2(a) and 2(b). One can see that n linearly changes with V_g with the rate dn/dV_g of about $(4.1 \pm 0.1) \times 10^{10}$ cm^{-2} V^{-1}. This rate is close to C/e, where C is the specific capacitance measured between the gate electrode and the 2D gas for the same structure. As seen, we were able to change the conductivity from $5\,G_0$ to $120\,G_0$ in our V_g range.

Because the heterostructures were grown on GaAs substrate with (013) surface orientation, it is natural to suppose that walls of the HgTe quantum well are not ideally planar and can be corrugated. For thin quantum wells (for our case the nominal quantum well width consists of only of 7–8 lattice constants)

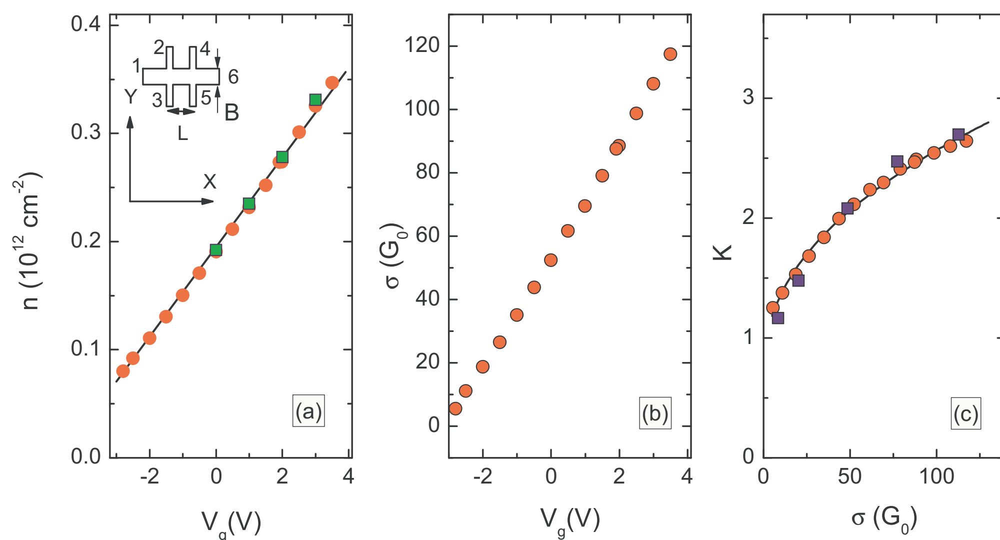

FIG. 2. (Color online) The gate voltage dependencies of (a) electron density and (b) conductivity obtained from the measurements on the standard Hall bar, shown in the inset. Circles and squares in (a) are data obtained from the Hall and SdH effect, respectively. (c) The conductivity dependencies of the conductivity anisotropy obtained from the measurements of nonlocal conductivity (squares) and from the measurements performed on the L-shaped Hall bar (circles). The lines are provided as a guide to the eye.

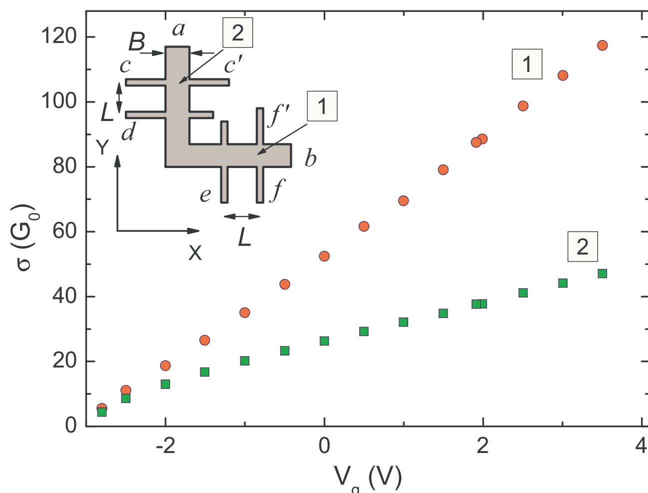

FIG. 3. (Color online) The gate voltage dependence of the conductivity measured on the different arms of the L-shaped Hall bar shown in the inset.

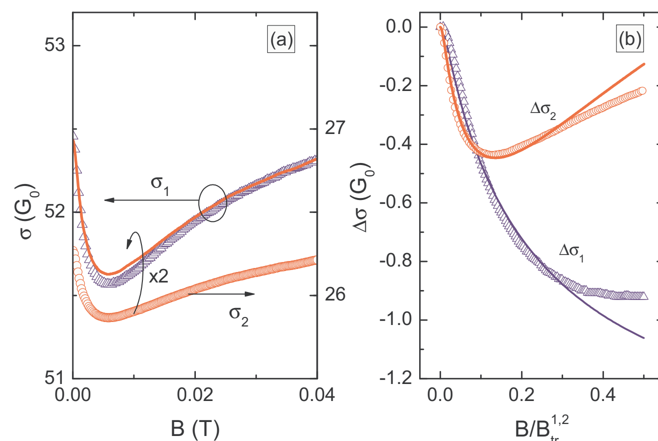

FIG. 4. (Color online) The dependencies of (a) $\sigma_{1,2}(B)$ and (b) $\Delta\sigma_{1,2}(B/B_{\rm tr}^{1,2})$ for the L-shaped Hall bar measured for $V_g = 0$ V at $T = 1.4$ K. $B_{\rm tr}^1 = 0.014$ T, $B_{\rm tr}^2 = 0.056$ T. The curve in (a) is $\sigma_2(B) \times K = \sigma_2(B)\sigma_1(0)/\sigma_2(0) = 2\,\sigma_2(B)$. The curves in (b) are the results of the best fit by Eq. (2) with the parameters given in the text.

such corrugation can result in the anisotropy of conductivity.[23] Therefore, let us consider the results concerning the conductivity anisotropy before analyzing the interference induced magnetoresistivity quantitatively. They have been obtained by two methods.

The first method is based on measurements of the nonlocal conductance on the standard Hall bar. When the principal axes x and y of the conductivity tensor coincide with axes X and Y of the sample coordinate system [see the inset in Fig. 2(a)] the conductivity anisotropy $K = \sigma_{xx}/\sigma_{yy}$ can be found from the ratio of nonlocal conductance (G_{nL}) to the local one (G_L):[24]

$$\frac{G_{nL}}{G_L} = \frac{4\sqrt{K}}{\pi} \exp\left(-\frac{L}{B}\frac{\pi}{\sqrt{K}}\right), \qquad (1)$$

where $G_L = I_{16}/V_{35}$ (or I_{16}/V_{24}), $G_{nL} = I_{23}/V_{45}$ with I_{ik} as the current flowing through the probes i and k, and V_{lm} as the voltage drop between the probes l and m.

The conductivity dependence of K measured by this method is plotted by squares in Fig. 2(c). It is seen that the conductivity anisotropy increases with the increase of the conductivity and electron density, and it reaches the value of $K \simeq 2.7$ at $\sigma = 120\,G_0$ ($n = 3.5 \times 10^{11}$ cm^{-2}). Of course, such a dependence may result from extended mechanical defects, such as scratches or notches, directed along the bar. To make sure that it is not the case and the anisotropy of the conductivity is the physical property of 2D electron gas in the structures investigated, we used the second method.

The anisotropy value in the second method is obtained from the measurements performed on the L-shaped Hall bar (see the inset in Fig. 3), which is made on the basis of the same wafer in such a way that the orientation of arm 1 on the wafer coincides with the orientation of the Hall bar shown in the inset in Fig. 2(a). Such measurements show that the electron densities in both arms are equal to each other with an accuracy better than 3%, but the conductivity of arm 1 ($\sigma_1 = I_{ab}/V_{ef} \times L/B = \sigma_{xx}$) is significantly higher than that of arm 2 ($\sigma_2 = I_{ab}/V_{cd} \times L/B = \sigma_{yy}$) as shown in Fig. 3. The ratio $\sigma_1/\sigma_2 = \sigma_{xx}/\sigma_{yy} = K$ plotted against the conductivity of arm 1 in Fig. 2(c) shows that the K values obtained by this method practically coincide with those obtained by the first method.

Thus, the conductivity of electron gas in the studied heterostructures with a narrow HgTe quantum well grown on (013) substrate is strongly anisotropic and should be taken into account with analysis of transport properties of such types of structures.

We are now in a position to consider the low field magnetoconductivity. The magnetic field dependence of σ_1 and σ_2 measured for both arms of the L-shaped Hall bar at $T = 1.4$ K and $V_g = 0$ V are presented in Fig. 4(a). Qualitatively these dependencies are analogous. The conductivity decreases in the low magnetic field, reaches the minimum near $B \simeq 60$ mT, and increases at higher magnetic field. Such behavior is typical for the interference induced magnetoconductivity for the case of relatively fast spin relaxation, when the spin relaxation time τ_s is close to or somewhat less than the phase relaxation time τ_ϕ. Notice that the magnitude of the magnetoconductivity $\Delta\sigma_1(B) = \sigma_1(B) - \sigma_1(0)$ and $\Delta\sigma_2(B) = \sigma_2(B) - \sigma_2(0)$ is different, whereas the characteristic magnetic field scales are the same; σ_2 being multiplied by a factor close to 2 coincides practically with σ_1 as illustrated by the solid line in Fig. 4(a).

Theoretically, the weak localization and antilocalization for narrow gap ($d \simeq d_c$) HgTe quantum wells is comprehensively studied in Ref. 15. The effective Bernevig-Hughes-Zhang (BHZ) Hamiltonian[5] is used to describe the spectrum of the 2D gas. The authors show that the run of magnetoconductivity curves is determined by four symmetry breaking rates connected to the specific of the energy band structure and disorder in addition to the phase relaxation rate. Obviously the fit of the smooth curve by the formula with five fitting parameters does not allow one to obtain these parameters reliably. Our numerical analysis (see Appendix A) shows that the well-known Hikami-Larkin-Nagaoka (HLN) expression[25,26]

$$\Delta\sigma(B) = G_0\mathcal{H}\left(\frac{B}{B_{tr}}, \frac{\tau}{\tau_\phi}, \frac{\tau}{\tau_s}\right), \qquad (2)$$

where

$$\mathcal{H}(b,x,y) = \psi\left(\frac{1}{2}+\frac{x+y}{b}\right) - \ln(x+y) + \frac{1}{2}\psi\left(\frac{1}{2}+\frac{x+2y}{b}\right) - \frac{1}{2}\ln(x+2y) - \frac{1}{2}\psi\left(\frac{1}{2}+\frac{x}{b}\right) + \frac{1}{2}\ln(x) - \psi\left(\frac{1}{2}+\frac{1}{b}\right)$$

can be used to obtain the phase relaxation time even in complicated systems such as HgTe quantum wells. It turns out that the $\Delta\sigma$ versus B curves calculated according to Ref. 15 are well fitted at relatively low magnetic field $b \lesssim 0.3$ by the HLN expression [Eq. (2)] for a wide range of parameters. What is more important for us, the phase relaxation time found from the fit coincides with that used in the calculation to better than 5% over the actual range of parameters. As for the τ_s value found from the fit, it is some combination of the other characteristic times and will not be analyzed in the present paper. Thus, the use of the HLN expression for obtaining the phase relaxation time from the magnetoconductivity curves is justified from our point of view.

In order to understand how it is important to take the conductivity anisotropy into account when obtaining the phase relaxation time, let us first analyze the data obtained on the two arms as if they have been obtained on two different samples with isotropic conductivity. The results of the best fit of experimental magnetoconductivity by Eq. (2) within the magnetic field range $B/B_{\rm tr}^{1,2} = 0 - 0.3$ ($B_{\rm tr}^1 = 0.014$ T, $B_{\rm tr}^2 = 0.056$ T) for each arm are presented in Fig. 4(b). The figure shows a good fit of the equation to the data. Nevertheless, the values of the fitting parameters are different. While the difference between the τ_ϕ values for arms 1 and 2 is not very large ($\tau_\phi^1 = 3.8 \times 10^{-11}$ s against $\tau_\phi^2 = 3.2 \times 10^{-11}$ s), the difference between τ_s^1 and τ_s^2 is significant: $\tau_s^1 = 0.9 \times 10^{-12}$ s is approximately five times smaller than $\tau_s^2 = 4.7 \times 10^{-12}$ s. In what follows we show that the reason for such a discrepancy is neglect of the conductivity anisotropy in the above data analysis.

The interference correction to the conductivity of the 2D anisotropic systems was studied in Refs. 27 and 28. If one follows this line of attack, the interference induced magnetoconductivity can be written within the diffusion approximation $\tau_\phi, \tau_s \gg \tau$ in the form

$$\Delta\sigma_{xx}(B) = \sqrt{K}\, G_0\, \mathcal{H}\left(\frac{B}{B'_{\rm tr}}, \frac{\tau'}{\tau_\phi}, \frac{\tau'}{\tau_s}\right),$$
$$\Delta\sigma_{yy}(B) = \frac{1}{\sqrt{K}}\, G_0\, \mathcal{H}\left(\frac{B}{B'_{\rm tr}}, \frac{\tau'}{\tau_\phi}, \frac{\tau'}{\tau_s}\right), \quad (3)$$

where $B'_{\rm tr} = \sqrt{B_{\rm tr}^1 B_{\rm tr}^2}$ and $\tau' = \sqrt{\tau_1 \tau_2}$.

Thus, the values of $\Delta\sigma_1/\sqrt{K}$ and $\Delta\sigma_2\sqrt{K}$ plotted as functions of $B/B'_{\rm tr}$ should coincide and they should be described by Eq. (2) with $b = B/B'_{\rm tr}$, $x = \tau'/\tau_\phi$, and $y = \tau'/\tau_s$. As evident from Fig. 5, the experimental data for arms 1 and 2 replotted in such a manner are really close to each other, but, what is more important, we obtain the very close parameters for two arms: $\tau_\phi = 3.8 \times 10^{-11}$ s, 3.5×10^{-11} s and $\tau_s = 3.1 \times 10^{-12}$ s, 3.2×10^{-12} s for arms 1 and 2, respectively. Existing differences between the data for different arms and between the corresponding fitting parameters may result from the fact that the diffusion regime $\tau \ll \tau_s, \tau_\phi$, is not strictly realized under our experimental conditions; τ_s is only 17 times larger than τ'.

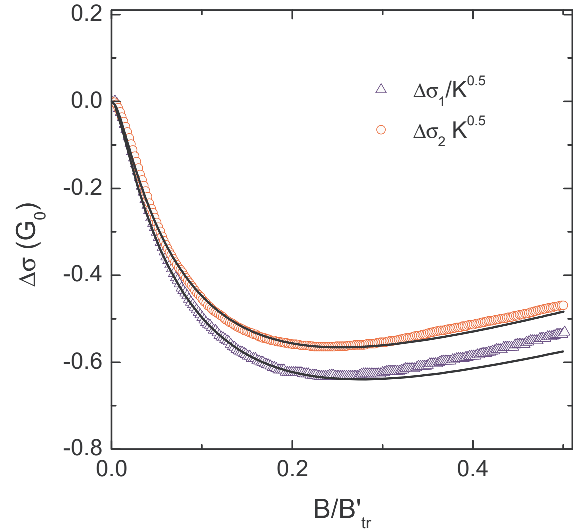

FIG. 5. (Color online) The values of $\Delta\sigma_1/\sqrt{K}$ and $\Delta\sigma_2\sqrt{K}$ plotted as functions of $B/B'_{\rm tr}$, $B'_{\rm tr} = 0.028$ T, for $V_g = 0$ V and $T = 1.4$ K. The symbols are the data and the solid lines are the result of the best fit by Eq. (2) with the parameters given in the text.

It is important to note here that the τ_ϕ values are very close to each other independent of how they have been obtained. Considering arms 1 and 2 as independent isotropic samples and taking into account the conductivity anisotropy, we have practically obtained the same results: $\tau_\phi = (3.2\text{–}3.8) \times 10^{-11}$ s. As for the spin relaxation time, the ignoring of the conductivity anisotropy when treating the data can give an error in τ_s of several times.

Strictly speaking, the above allowance for the conductivity anisotropy is rigorous in the case when the electric current flows along the principal axes of the conductivity tensor. In Appendix B we show that the measurements performed on the L-shaped Hall bar allows one to find the principal exes of the conductivity tensor and, thus, perform the analysis of the magnetoconductivity for the arbitrary orientation of the bar and conductivity tensor. It is shown that misorientation between the conductivity tensor and the Hall bar is small enough so that taking it into account is not needed in our concrete case.

Now, making sure that Eq. (3) for the interference correction in the anisotropic 2D system describes the experimental data adequately we can proceed to the analysis of the dependencies of the parameters τ_ϕ and τ_s on the temperature and conductivity.

The temperature dependencies of τ_ϕ and τ_s for two gate voltages are depicted in Fig. 6. One can see that the T dependencies of τ_ϕ obtained for each of the arms coincide very closely. They are well described by the $1/T$ law that is consistent with the theoretical prediction for the case when the phase relaxation is determined by the inelasticity of the electron-electron (e-e) interaction.[29] The "spin" relaxation time is practically independent of the temperature as it should

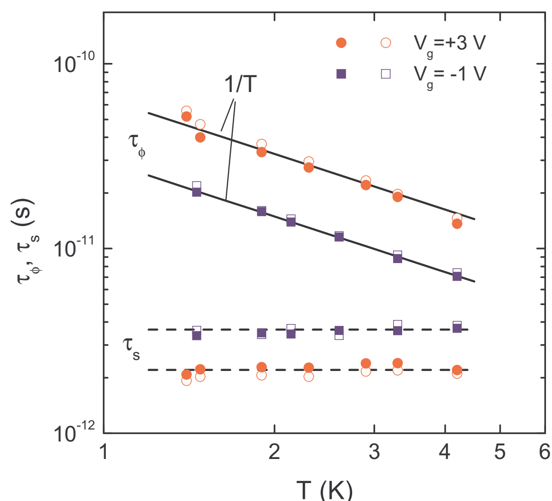

FIG. 6. (Color online) The temperature dependencies of τ_ϕ and τ_s for two gate voltages $V_g = -1$ and 3 V. Solid and open symbols plot the data obtained from analysis of the dependencies $\Delta\sigma_1(B)/\sqrt{K}$ and $\Delta\sigma_2(B)\sqrt{K}$, respectively. The dashed lines are provided as a guide to the eye.

be for the degenerate gas of carriers. Such dependencies of the fitting parameters τ_ϕ and τ_s support using of the HLN expression for description of interference induced magnetoresistance.

Let us now consider the main result of the paper. It is the conductivity dependence of the phase relaxation time shown in Fig. 7, where $\sigma' = \sqrt{\sigma_1\sigma_2}$. It is evident that τ_ϕ found experimentally increases with the increasing conductivity. Such a behavior is analogous to that observed in quantum wells with ordinary spectrum (see, e.g., Ref. 30, where the data for the GaAs/$In_{0.2}Ga_{0.8}As$/GaAs quantum well are presented). Our data are in satisfactory agreement with the theoretical results obtained in Ref. 18 for the usual 2D systems for the case when inelasticity of *e-e* interaction is the main mechanism of phase relaxation. This is clearly seen in Fig. 7, where the curves represent the calculation results for two values of the parameter *e-e* interaction F_0^σ: $F_0^\sigma = 0$ and -0.5. Note the fact that most of the experimental points falling between the theoretical curves cannot be regarded as a method of determining F_0^σ vs σ dependence in these systems.

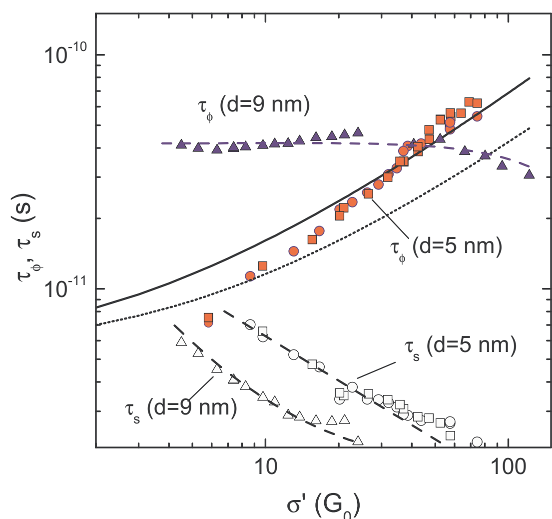

FIG. 7. (Color online) The conductivity dependence of τ_ϕ and τ_s for the HgTe quantum well with inverted ($d = 9$ nm) and normal ($d = 5$ nm) energy spectrum obtained in Ref. 17 and this paper, respectively. The solid and dotted lines are calculated according to Ref. 18 with $F_0^\sigma = 0$ and -0.5, respectively. The dashed lines are provided as a guide to the eye.

The growing τ_ϕ vs σ dependence observed in the present paper for the narrow quantum well, $d = 5$ nm, with normal energy spectrum differs drastically from that obtained in Ref. 17 by the same method for the structures with the wider quantum well, $d = (9–10)$ nm, with the inverted subband ordering. The results from Ref. 17 are presented in Fig. 7 also. As seen, τ_ϕ is practically independent of the conductivity in the quantum well with inverted spectrum in contrast to the data obtained for the wells with normal spectrum.

Thus, the fitting parameter τ_ϕ identifying with the phase relaxation time behaves itself with increasing σ in a narrow quantum well HgTe with normal subband ordering in the same way as in the usual 2D systems. When we are dealing with electrons in the inverted band, the τ_ϕ vs σ behavior is extraordinary. One of the possible reasons for the latter case is that the fitting parameters τ_ϕ may not correspond to the true phase relaxation time despite the fact that the experimental magnetoconductivity curves are fitted to the theoretical formula rather well. The theory of weak localization and antilocalization based on the effective 2D BHZ Hamiltonian works in the vicinity of critical width d_c only. Quite apparently for the quantum wells with $d = 9–10$ nm and larger such approximation is rough enough, and a more refined theory of weak localization based on the multiband Kane Hamiltonian should be developed.

IV. CONCLUSION

This paper presents the results of an experimental study of the interference quantum correction to the conductivity in the narrow quantum well HgTe with a normal energy spectrum. Analysis of the interference induced low-field magnetoconductivity has been performed by taking account the conductivity anisotropy. We have shown that the phase relaxation time found from the fit of the magnetoconductivity curves increases with the conductivity increase analogously to that observed in ordinary single quantum wells. Such behavior is in agreement with that predicted theoretically for the case when inelasticity of the *e-e* interaction is the main mechanism of the phase relaxation time. At the same time, it differs markedly from the behavior of τ_ϕ obtained in the wider HgTe quantum wells with the inverted energy spectrum, where τ_ϕ remains nearly constant over the wide conductivity range.[17] We believe that the different structure of the multicomponent electron wave functions could be responsible for the different τ_ϕ vs σ behavior in the HgTe quantum wells with the inverted and normal spectra.

ACKNOWLEDGMENTS

We are grateful to I. V. Gornyi for numerous illuminating discussions. This work has been supported in part by the RFBR

(Grants No. 11-02-12126, No. 12-02-00098, and No. 13-02-00322).

APPENDIX A

In Ref. 15 the weak localization in HgTe quantum well is studied theoretically near the critical width $d = d_c$. Analysis is based on the effective 2D BHZ Hamiltonian derived from symmetrical grounds,[5] which results in the following dispersion $E(k)$:

$$E_\pm(k) = Dk^2 \pm \sqrt{A^2k^2 + m^2(k)}, \tag{A1}$$

$$m(k) = M + Bk^2. \tag{A2}$$

Two signs correspond to the electron and hole bands. Material dependent parameters A, B, and D are positive with $B > D$. The parameter M is positive at $d < d_c$ and negative at $d > d_c$, $|2M|$ is the gap between conduction and valence band [see Fig. 1(c)]. Two expressions, Eqs. (37) and (65), for the magnetic field dependence of the conductivity due to suppression of the interference quantum corrections have been derived within the framework of the diffusion approximation for two limiting cases. The first of these expressions is obtained for the situation when the Fermi energy is in the range of almost linear spectrum. The second one relates to the case when the Fermi level lies close to the bottom (top) of the electron (hole) subband, where the spectrum is practically parabolic. Here we use a more general formula,[31] which covers the whole energy range:

$$\Delta\sigma = G_0\left[\ln\left(\frac{\tau}{\tau_\phi}+\frac{\tau}{\tau_A}+\frac{\tau}{\tau_{SO}}\right) - \ln\left(\frac{\tau}{\tau_\phi}+\frac{\tau}{\tau_m}+\frac{\tau}{\tau_{SO}}\right) + \frac{1}{2}\ln\left(\frac{\tau}{\tau_\phi}+\frac{\tau}{\tau_{SO}}\right) - \frac{1}{2}\ln\left(\frac{\tau}{\tau_\phi}\right)\right]. \tag{A3}$$

In Eq. (A3) the Dresselhaus-type splitting of spectrum is neglected, i.e., the corresponding rate $1/\tau_\Delta = 0$ is set equal to zero.[15] It is a good approximation if the Fermi energy is not much greater than the gap width $|2M|$ that is the case.

There are three symmetry breaking rates in Eq. (A3): $1/\tau_{SO}$, $1/\tau_A$, and $1/\tau_m$. The first describes the weak block mixing in the BHZ Hamiltonian. It is present for an arbitrary position of the Fermi energy and is assumed to be smaller than $1/\tau$. Near the band bottom (and for very high energies, where the spectrum is no longer linear) the rates $1/\tau_m$ and $1/\tau_A$ satisfy $\tau/\tau_m \simeq 1$, while $\tau/\tau_A \ll 1$. In the region of the linear spectrum the relations are opposite: $\tau/\tau_m \ll 1$, while $\tau/\tau_A \simeq 1$. If one introduces the quantity $\varepsilon = (E_F - Bk_F^2)/Ak_F$, where E_F is the Fermi energy measured from the bottom (top) of the electron (hole) band, and takes into account that $Dk^2 \ll E_F$ in our case, the rates $1/\tau_m$ and $1/\tau_A$ can be estimated as follows:[31,32]

$$\frac{\tau}{\tau_m} \simeq \frac{(1-\varepsilon^2)^2}{2\varepsilon^2} \tag{A4}$$

for $\varepsilon > (\sqrt{3}-1)/\sqrt{2} \simeq 0.52$ and $\tau/\tau_m = 1$ otherwise,

$$\frac{\tau}{\tau_A} \simeq \varepsilon^4. \tag{A5}$$

Equations (A4) and (A5) are more refined versions of Eqs. (39) and (60) from Ref. 15.

As for τ_{SO} in Eq. (A3), it is responsible both for the effect of short-range impurity within the quantum well and for the Rashba effect due to asymmetry of the quantum well. For the symmetric quantum well, the following rough estimate can be applied:

$$\frac{\tau}{\tau_{SO}} \simeq \left(\frac{Pk_F}{E_g}\right)^2, \tag{A6}$$

where P and E_g stand for the Kane matrix element and the energy gap in HgTe, respectively.

The expression for the magnetic field dependence of the conductivity due to suppression of the weak localization $\Delta\sigma(b)$ is obtained from Eq. (A3) if one replaces logarithms by the digamma functions according to the rule

$$\ln x \to \psi\left(\frac{1}{2}+\frac{x}{b}\right) - \psi\left(\frac{1}{2}+\frac{1}{b}\right) - \ln x. \tag{A7}$$

In order to justify the correctness of the use of the HLN expression[25] to obtain the phase relaxation time in our case, we have calculated the set of the magnetoconductivity curves using the above expressions and the following parameters of the effective Hamiltonian obtained by extrapolation to $d = 5$ nm of data from Ref. 33: $A = 4$ eV Å, $B = 43$ eV Å^2, $D = 23$ eV Å^2, and $M = 0.012$ eV. The τ to τ_ϕ ratio was in the range from 0.005 to 0.1 that includes the actual one. Shown in Fig. 8(a) are the $\Delta\sigma$ vs b plots calculated from Eqs. (A3) and (A7) for different positions of the Fermi level in the conduction band for $\tau/\tau_\phi = 0.005$. The results of the best fit by the HLN expression made at $b < 0.3$ are presented in this figure as well. As seen, the fit quality is fine. An important point is that the fitting τ/τ_ϕ value is very close to that substituted in Eqs. (A3) and (A7). The maximal deference is about 20% as seen from Fig. 8(b), it is achieved when the Fermi level is near the conduction band bottom. For the actual case of $E_F = (25–55)$ meV, the fitting and substituted τ/τ_ϕ values

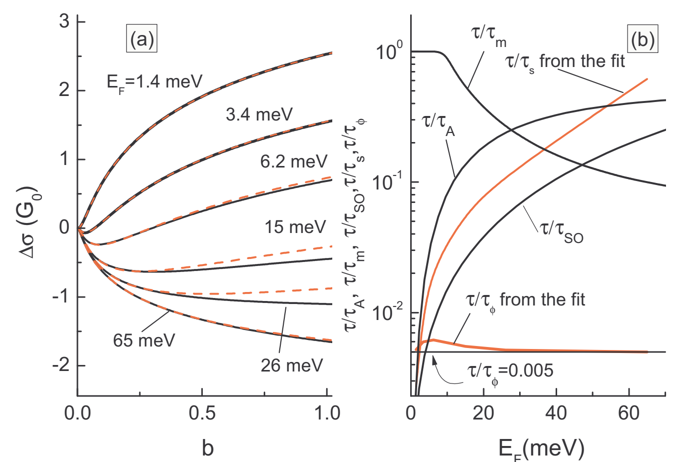

FIG. 8. (Color online) (a) The solid lines are the dependence $\Delta\sigma(b)$ calculated from Eqs. (A4) and (A7) for different Fermi energies with parameters shown in (b) and $\tau/\tau_\phi = 0.005$. The dashed lines are the results of the best fit performed at $b < 0.3$ by the HLN expression. (b) The parameters τ/τ_m, τ/τ_A, and τ/τ_{SO} calculated from Eqs. (A4)–(A6), and the fitting parameters τ/τ_s and τ/τ_ϕ plotted as a function of the Fermi energy.

practically coincide. As for the fitting τ/τ_s value, the fit gives some effective characteristic time. It corresponds neither to τ/τ_m, τ/τ_A, nor to τ/τ_{SO}, although it behaves itself with the growing Fermi energy analogously to τ/τ_A and τ/τ_{SO}. Close results have been obtained for $d = 5.5$–7.0 nm with a set of parameters from Ref. 33 within the τ/τ_ϕ range from 0.005 to 0.1.

APPENDIX B

Analysis in the paper is performed under assumption that the principal axes x and y of the conductivity tensor coincide with the axes X and Y of the coordinate system connected with the sample. If it is not the case, i.e., the angle θ between the X and x axes is nonzero (see the inset in Fig. 9), the σ_{xx} and σ_{yy} components as well as the θ angle can be found from resolving the following system of equations:

$$\begin{aligned} \sigma_1^{-1} &= \sigma_{xx}^{-1}(\cos\theta)^2 + \sigma_{yy}^{-1}(\sin\theta)^2, \\ \sigma_2^{-1} &= \sigma_{xx}^{-1}(\sin\theta)^2 + \sigma_{yy}^{-1}(\cos\theta)^2, \\ V_{cc'} &= \tfrac{1}{2} I_{ab}\left(\sigma_{xx}^{-1} - \sigma_{yy}^{-1}\right)\sin 2\theta, \\ V_{f'f} &= V_{cc'}, \end{aligned} \tag{B1}$$

where the current I_{ab} flowing through the probes a and b, and the quantities σ_1, σ_2, and $V_{cc'}$ (or $V_{f'f}$) are measured experimentally. Doing so we have obtained $\theta = (22 \pm 5)^\circ$, and σ_{xx}, σ_{yy} plotted against the gate voltage in Fig. 9. One can see that the data obtained are consistent with the results obtained in Sec. III; $\sigma_{xx} > \sigma_1$ while $\sigma_{yy} < \sigma_2$ so that $\sigma_{xx}/\sigma_{yy} > \sigma_1/\sigma_2$.

As for the interference induced magnetoconductivity measured on the L-shaped Hall bar, it is easy to show that the following expression is valid for $\Delta\sigma_{1,2}(B)$:

$$\begin{aligned} \Delta\sigma_1(B) &= \sqrt{\frac{\sigma_1}{\sigma_2}}\, G_0\, \mathcal{H}\left(\frac{B}{B'_{tr}}, \frac{\tau'}{\tau_\phi}, \frac{\tau'}{\tau_s}\right) F(K,\theta), \\ \Delta\sigma_2(B) &= \sqrt{\frac{\sigma_2}{\sigma_1}}\, G_0\, \mathcal{H}\left(\frac{B}{B'_{tr}}, \frac{\tau'}{\tau_\phi}, \frac{\tau'}{\tau_s}\right) F(K,\theta), \end{aligned} \tag{B2}$$

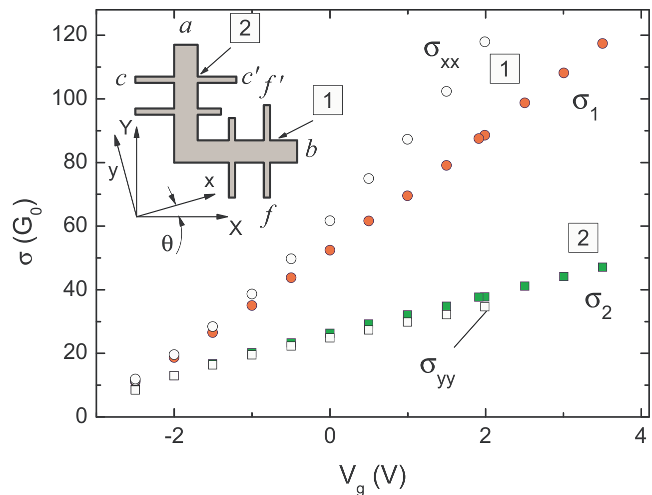

FIG. 9. (Color online) The gate voltage dependence of σ_1 and σ_2 measured for arms 1 and 2 (solid symbols) as compared to that of σ_{xx} and σ_{yy}, found as described in the text. The inset illustrates the orientation of the principal axes x and y of the conductivity tensor in the coordinate system of the sample.

where $K = \sigma_{xx}/\sigma_{yy}$ and

$$F(K,\theta) = \sqrt{\frac{K}{(\sin^2\theta + K\cos^2\theta)(K\sin^2\theta + \cos^2\theta)}}. \tag{B3}$$

Thus, the experimental dependencies $\Delta\sigma_1(B)\sqrt{\sigma_2/\sigma_1}$ and $\Delta\sigma_2(B)\sqrt{\sigma_1/\sigma_2}$ measured for arbitrary orientation of the L-shaped Hall should be described by the same function $\mathcal{H}(b,x,y)$ multiplied by the factor $F(K,\theta)$ given by Eq. (B3).

If one uses $\theta = 22^\circ$ and maximal under our conditions value of K, $K = 4$, one obtains $F(K,\theta) \simeq 0.9$. Because this value is close to one, it is obvious that ignoring $F(K,\theta)$ in the main text does not affect the results of the paper. It is justified by the direct inclusion of the factor $F(K,\theta)$ into the fitting procedure. Taking the factor $F(K,\theta)$ into account results in the maximal increase of τ_ϕ by approximately 2% and a decrease of τ_s by 20% or less over the entire temperature and conductivity ranges used in the paper.

[1] V. A. Volkov and T. N. Pinsker, Zh. Eksp. Teor. Fiz. **70**, 2268 (1976) [Sov. Phys. JETP **43**, 1183 (1976)].
[2] M. I. Dyakonov and A. Khaetskii, Zh. Eksp. Teor. Fiz. **82**, 1584 (1982) [Sov. Phys. JETP **55**, 917 (1982)].
[3] Y. R. Lin-Liu and L. J. Sham, Phys. Rev. B **32**, 5561 (1985).
[4] L. G. Gerchikov and A. Subashiev, Phys. Status Solidi B **160**, 443 (1990).
[5] B. A. Bernevig, T. L. Hughes, and S.-C. Zhang, Science **314**, 1757 (2006).
[6] G. Landwehr, J. Gerschütz, S. Oehling, A. Pfeuffer-Jeschke, V. Latussek, and C. R. Becker, Physica E **6**, 713 (2000).
[7] X. C. Zhang, A. Pfeuffer-Jeschke, K. Ortner, C. R. Becker, and G. Landwehr, Phys. Rev. B **65**, 045324 (2002).
[8] K. Ortner, X. C. Zhang, A. Pfeuffer-Jeschke, C. R. Becker, G. Landwehr, and L. W. Molenkamp, Phys. Rev. B **66**, 075322 (2002).
[9] X. C. Zhang, K. Ortner, A. Pfeuffer-Jeschke, C. R. Becker, and G. Landwehr, Phys. Rev. B **69**, 115340 (2004).
[10] M. König, S. Wiedmann, C. Brüne, A. Roth, H. Buhmann, L. W. Molenkamp, X.-L. Qi, and S.-C. Zhang, Science **318**, 766 (2007).
[11] G. M. Gusev, Z. D. Kvon, O. A. Shegai, N. N. Mikhailov, S. A. Dvoretsky, and J. C. Portal, Phys. Rev. B **84**, 121302 (2011).
[12] Z. D. Kvon, E. B. Olshanetsky, E. G. Novik, D. A. Kozlov, N. N. Mikhailov, I. O. Parm, and S. A. Dvoretsky, Phys. Rev. B **83**, 193304 (2011).
[13] G. Tkachov and E. M. Hankiewicz, Phys. Rev. B **84**, 035444 (2011).
[14] J. W. Nicklas and J. W. Wilkins, Phys. Rev. B **84**, 121308 (2011).

[15] P. M. Ostrovsky, I. V. Gornyi, and A. D. Mirlin, Phys. Rev. B **86**, 125323 (2012).

[16] E. B. Olshanetsky, Z. D. Kvon, G. M. Gusev, N. N. Mikhailov, S. A. Dvoretsky, and J. C. Portal, Pis'ma Zh. Eksp. Teor. Fiz. **91**, 375 (2010) [JETP Lett. **91**, 347 (2010)].

[17] G. M. Minkov, A. V. Germanenko, O. E. Rut, A. A. Sherstobitov, S. A. Dvoretski, and N. N. Mikhailov, Phys. Rev. B **85**, 235312 (2012).

[18] G. Zala, B. N. Narozhny, and I. L. Aleiner, Phys. Rev. B **64**, 214204 (2001).

[19] N. N. Mikhailov, R. N. Smirnov, S. A. Dvoretsky, Y. G. Sidorov, V. A. Shvets, E. V. Spesivtsev, and S. V. Rykhlitski, Int. J. Nanotechnol. **3**, 120 (2006).

[20] V. A. Larionova and A. V. Germanenko, Phys. Rev. B **55**, 13062 (1997).

[21] X. C. Zhang, A. Pfeuffer-Jeschke, K. Ortner, V. Hock, H. Buhmann, C. R. Becker, and G. Landwehr, Phys. Rev. B **63**, 245305 (2001).

[22] E. G. Novik, A. Pfeuffer-Jeschke, T. Jungwirth, V. Latussek, C. R. Becker, G. Landwehr, H. Buhmann, and L. W. Molenkamp, Phys. Rev. B **72**, 035321 (2005).

[23] It should be mentioned that not only the corrugation of the HgTe/$Hg_{1-x}Cd_xTe$ interfaces may result in the conductivity anisotropy. Anisotropy can be of technological origin. For instance, the quasiperiodic structure of different composition of solid solution $Hg_{1-x}Cd_xTe$ can be formed during epitaxial growth under certain conditions as shown in Ref. 34. This modulated composition can also result in anisotropy of electrical properties.

[24] A. V. Germanenko and G. M. Minkov, Solid State Commun. **74**, 649 (1990).

[25] S. Hikami, A. I. Larkin, and Y. Nagaoka, Prog. Theor. Phys. **63**, 707 (1980).

[26] W. Knap, A. Zduniak, L. H. Dmowski, S. Contreras, and M. I. Dyakonov, Phys. Status Solidi B **198**, 267 (1996).

[27] P. Wölfle and R. N. Bhatt, Phys. Rev. B **30**, 3542 (1984).

[28] R. N. Bhatt, P. Wölfle, and T. V. Ramakrishnan, Phys. Rev. B **32**, 569 (1985).

[29] B. L. Altshuler and A. G. Aronov, in *Electron-Electron Interaction in Disordered Systems*, edited by A. L. Efros and M. Pollak (North Holland, Amsterdam, 1985), p. 1.

[30] G. M. Minkov, A. V. Germanenko, and I. V. Gornyi, Phys. Rev. B **70**, 245423 (2004).

[31] I. V. Gornyi (private communication).

[32] I. V. Gornyi, V. Y. Kachorovskii, and P. M. Ostrovsky (unpublished).

[33] X.-L. Qi and S.-C. Zhang, Rev. Mod. Phys. **83**, 1057 (2011).

[34] I. Sabinina, A. Gutakovsky, Y. G. Sidorov, and A. Latyshev, Pis'ma Zh. Eksp. Teor. Fiz. **94**, 348 (2011) [JETP Letters **94**, 324 (2011)].